Biophysical Journal, Volume *114*

Supplemental Information

The Antiparallel Dimerization of Myosin X Imparts Bundle Selectivity for Processive Motility

Matthew A. Caporizzo, Claire E. Fishman, Osamu Sato, Ryan M. Jamiolkowski, Mitsuo Ikebe, and Yale E. Goldman

Supplemental Information for

The Antiparallel Dimerization of Myosin X Imparts Bundle Selectivity for Processive Motility

Matthew A. Caporizzo[1], Claire E. Fishman[1], Osamu Sato[2], Ryan M Jamiolkowski[1], Mitsuo Ikebe[2], Yale E. Goldman[1]

[1]*Department of Physiology, Pennsylvania Muscle Institute, University of Pennsylvania School of Medicine*
[2]*Department of Cellular and Molecular Biology, University of Texas Health Northeast*

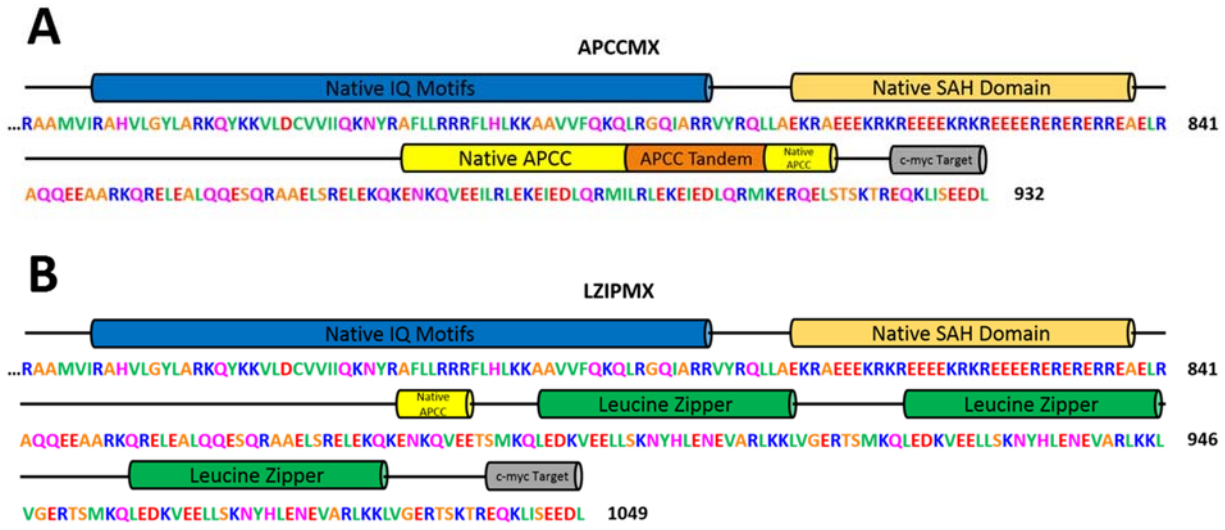

Figure S1. A, sequence diagram for the APCCMX construct. Stable dimers with the native (antiparallel) orientation were formed by the addition of a repeat native dimerization motif in tandem following the single stable α-helical segment (SAH). B, sequence diagram for the LZIPMX construct. Parallel dimers of HMM Myosin X were formed by addition of a repeated leucine zipper coiled-coil motif (green). Amino acid colors: orange: small non-polar, green: hydrophobic, magenta: polar, Red: acidic, blue: basic.

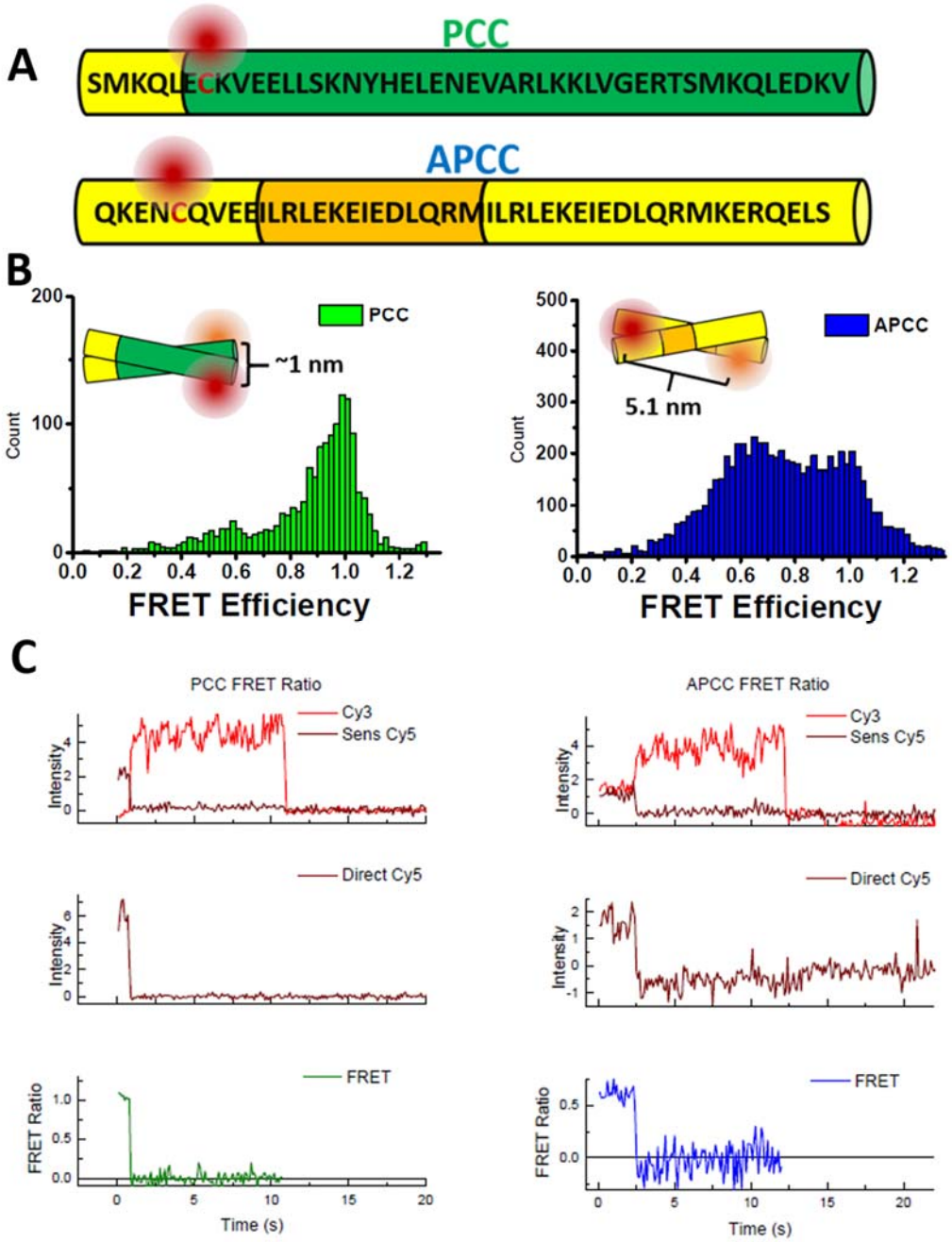

Figure S2. Single molecule FRET data from purified dimerization domains of myosin X. A. Schematic showing the two coiled coils utilized for dimerization of myosin X (APCCMX, left and LZIPMX, right), where a single residue in the sequence has been changed to cysteine to enable fluorescent labeling (shown in red). B. FRET efficiency histograms of the leucine zipper (green) and the extended native coiled-coil motif (blue). C. Representative FRET traces from the leucine zipper (left) and the extended native coiled-coil (blue) motifs. Top row, recordings of Cy3 and sensitized Cy5 (FRET) fluorescence intensity as a function of time. Middle row, direct Cy5 intensity (confirmation of FRET pair co-localization and Cy5 bleaching). Bottom row, FRET ratio. Traces were selected which show clear Cy5 bleaching (middle row) correlated with an increase in Cy3 intensity (top row) and a clear single-step Cy3 bleach which confirmed the presence of Cy3/Cy5 single molecule FRET.

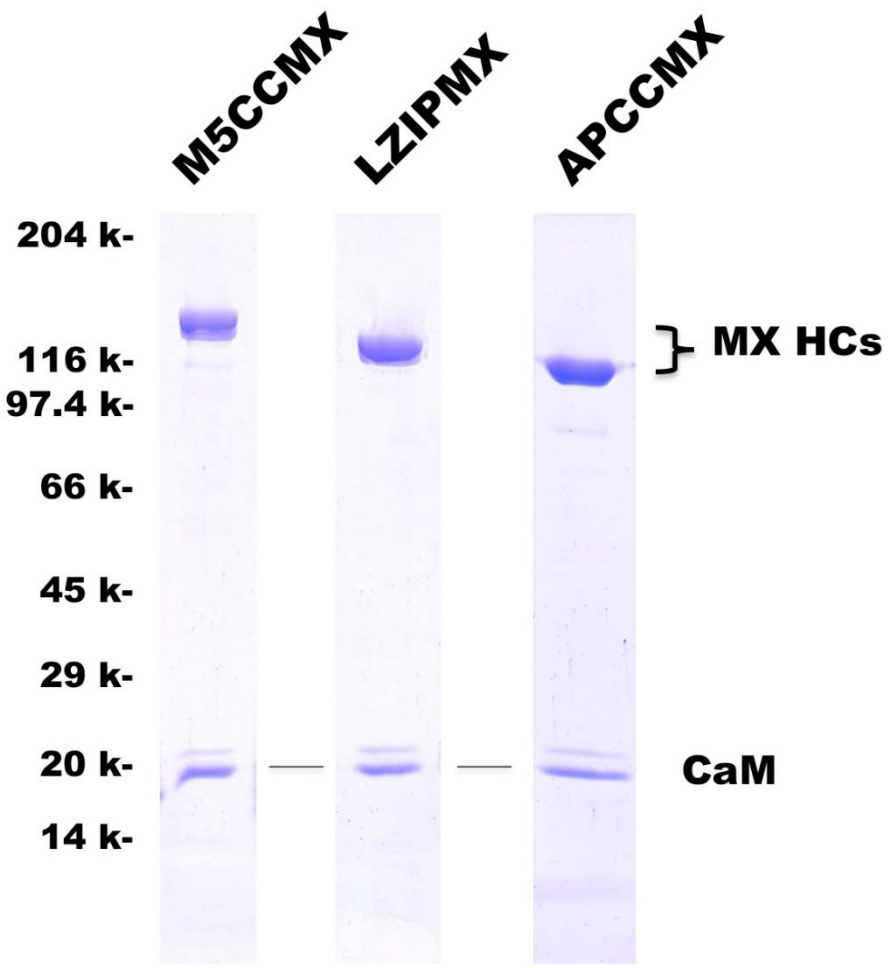

Figure S3: SDS-Page gel of myosin heavy chains and the calmodulin band. From left to right, MVCCMX, LZIPMX, and APCCMX, the heavy chain to CaM ratios, according to calibrated gels, are, 2.8 ± 0.31, 2.8 ± 0.4, and 3.0 ± 0.035 respectively (CaM:myosin heavy chain ratio ± S.E.M. from at least 3 measurements).

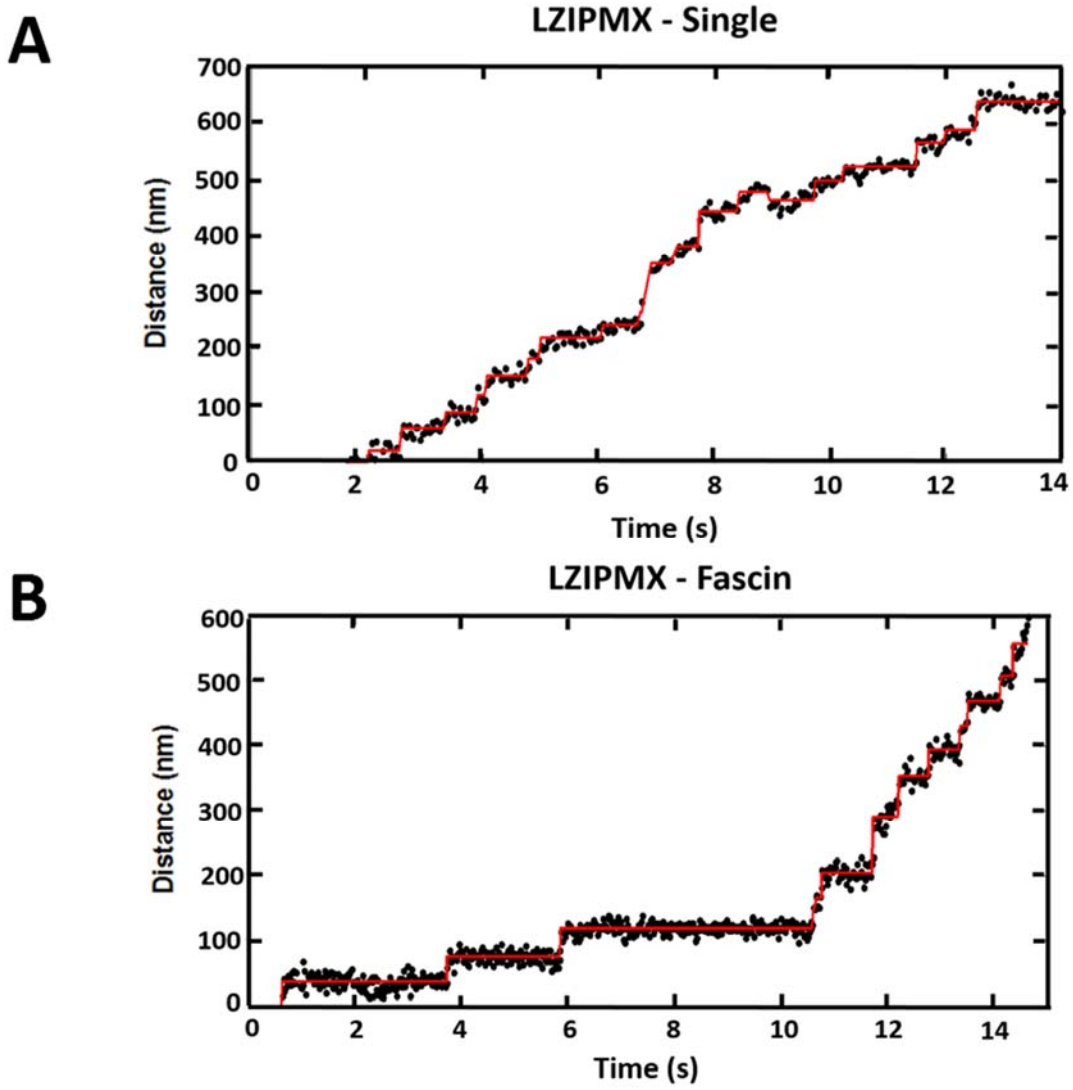

Figure S4. A, representative traces for LZIPMX on single actin and, B, fascin-bundled actin at 500 nM ATP. Black points are the position along the actin filament or bundle. The red lines are the output of the step-finding algorithm.

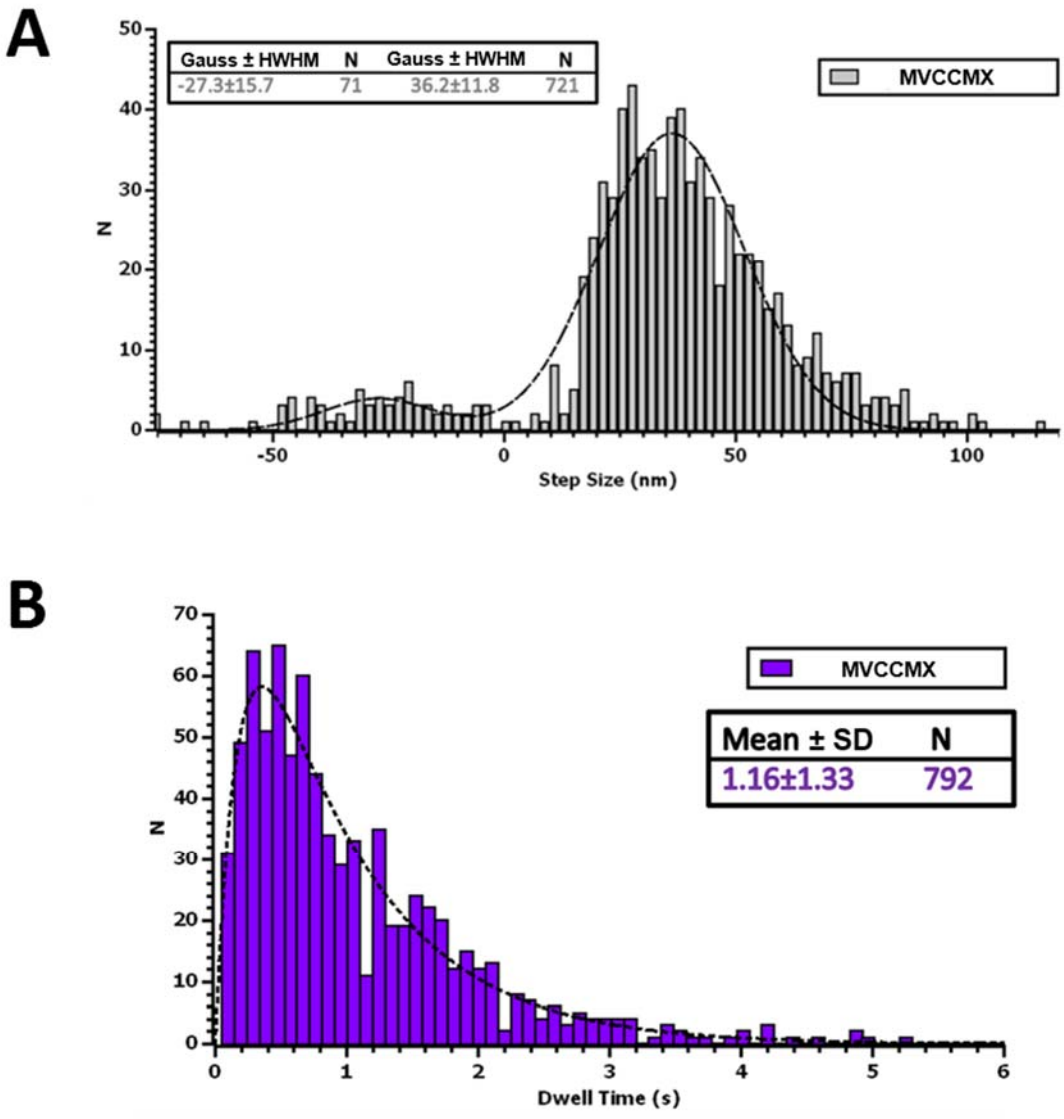

Figure S5. A, step size distribution for MVCCMX on single actin filaments at 500nM ATP. Best fit to double Gaussian distribution (single forward and backward stepping peaks). 721 forward steps and 71 backwards steps were analyzed. B, Dwell time distribution for MVCCMX on single actin filaments at 500nM ATP. Dashed line, best fit to double exponential distribution. Neither average step size nor average dwell time are significantly different from those of LZIPMX measured in this paper.

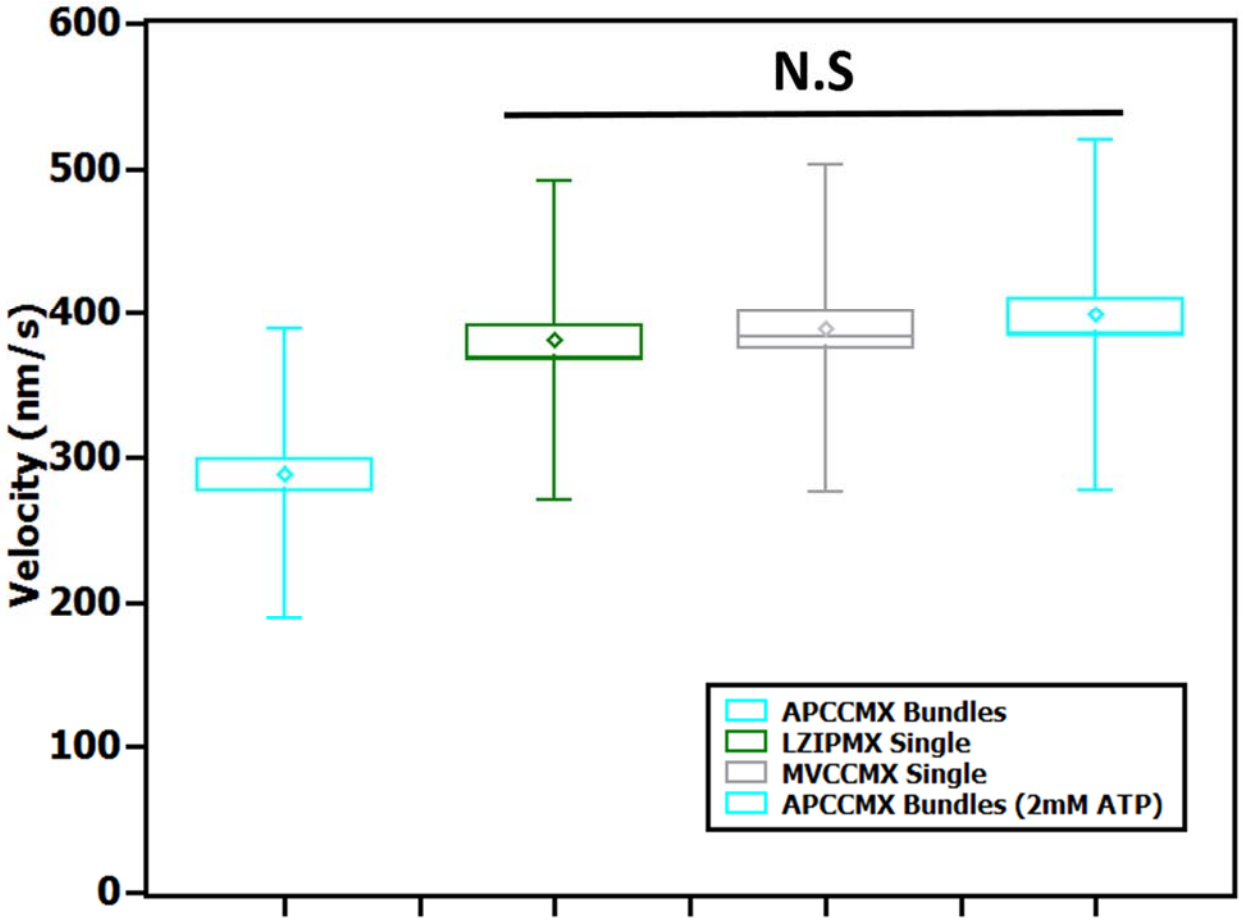

Figure S6. Velocity at saturating [ATP]. The saturating velocity was not different between APCCMX and the parallel myosin X constructs. The first 3 box plots are velocities at 500 μM [MgATP]. The far right box plot is APCCMX at 2 mM [ATP] where velocity has saturated for APCCMX on fascin-actin bundles. Velocity of APCCMX on single filaments was not measured at saturating [MgATP] due to insufficient processivity. Each box represents N > 100 runs.

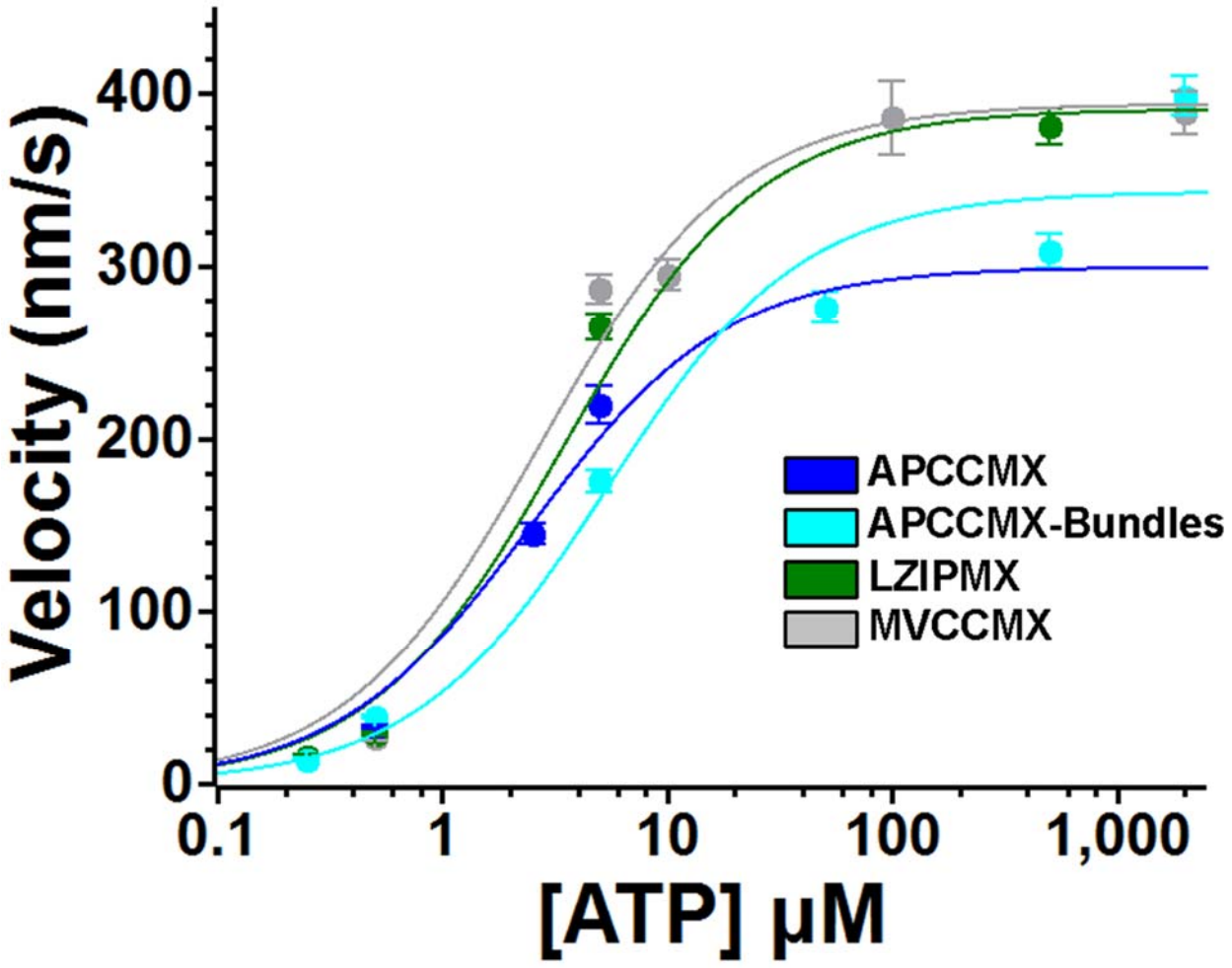

Figure S7. Velocity vs. [MgATP]. The velocity of myosin X increases with concentration of MgATP and saturates at 100-500 μM. Data points represent the average velocity from 1-3 experiments and n >50 trajectories per experiment. Error bars are S.E.M.s. Solid lines are the fit to Eq. 2 in the text, fitted parameters are listed in Table 1. V_{MAX} was set to 300 nm/s for plotting the APCCMX curve for single filaments (blue) because processive runs were not observed at saturating [MgATP].

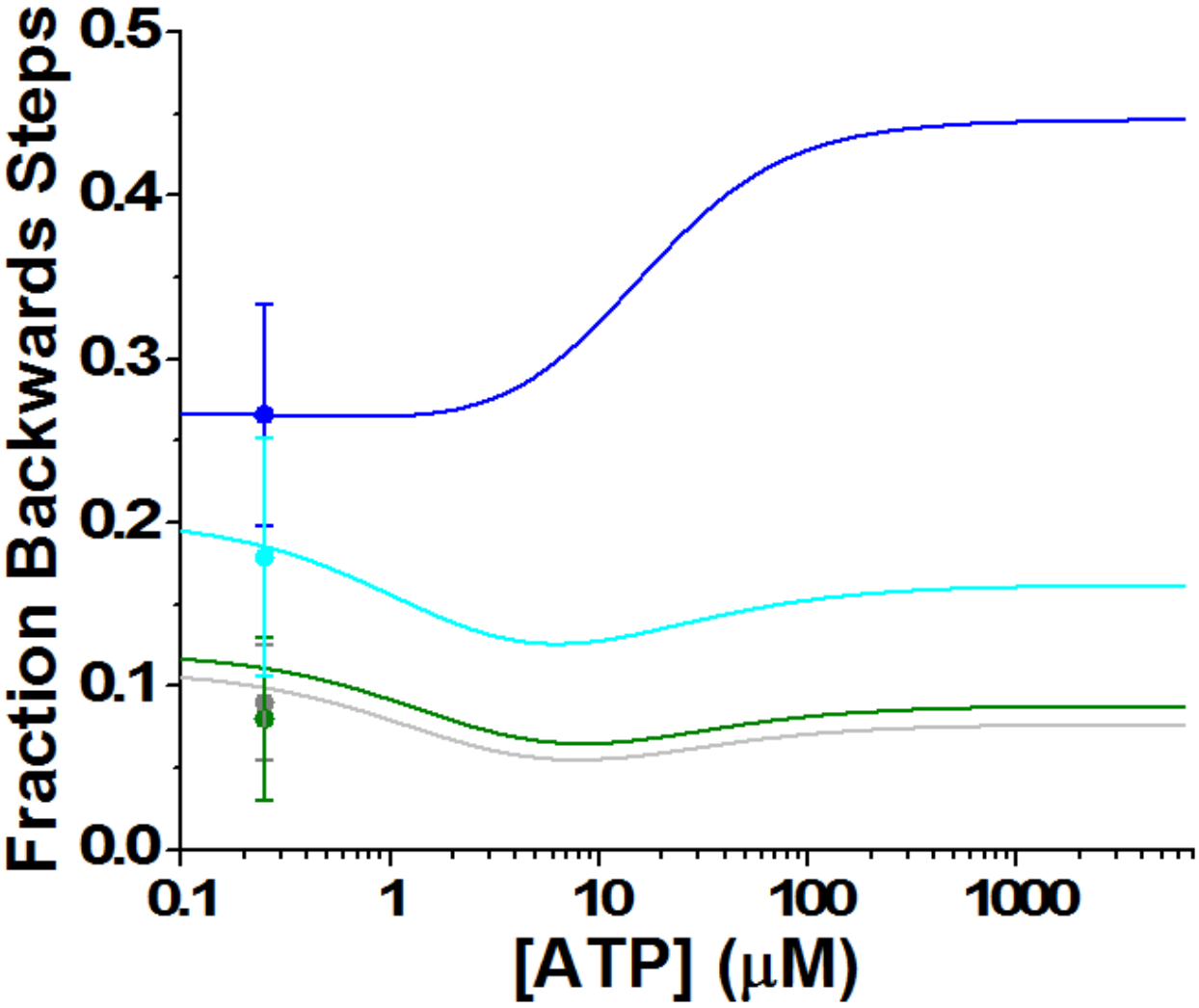

Figure S8. Proportion of backwards stepping vs. [MgATP]. Data points are the experimentally measured fraction of backwards steps at 500 nM ATP ± S.D.s. Solid lines are backwards steps predicted by the mathematic model outlined in the text which also incorporated run length and velocity as constraints. The model predicts that the fraction of backwards steps changes with [MgATP] as shown.

Mathematical Model:

The transition of the dimer through biochemically distinguishable states represents a Markov chain: a random process undergoing memory-less state transitions in which the relative probability of transitioning into another state depends only on the current state. To track forward or backward translocation events, the physical position on the actin filament must be distinguished. Four binding sites on the actin filament, α – δ in Fig. 5, define 11 unique states in the Markov chain and four additional states (identified with boxes) correspond to completion of a forward (A_2 or B_2) or reverse (A_0 or B_0) translocation event. When the molecule completes a hydrolysis cycle, it returns to the corresponding original biochemical state (i.e. A_1 or B_1). If the construct enters state G, the run has terminated.

This model enables generating a Markov matrix which defines the probability of transition from between two states relative to the (unitary) total probability of transition into all accessible states (37). Note that the Markov matrix does not contain rate constants but instead contains relative probabilities on each transition, determined by the relative reaction rates. The average dwell time in a state is given by the reciprocal of the total of all transition rates from that state into its accessible states.

$k_{ADPoff\text{-}rear}$ (s^{-1})	$k_{ADPoff\text{-}front}$ (s^{-1})	$k_{ATPon\text{-}rear}$ ($\mu M^{-1}s^{-1}$)	$k_{ATPon\text{-}front}$ ($\mu M^{-1}s^{-1}$)	$k_{rebind\text{-}for}$ (s^{-1})	$k_{rebind\text{-}back}$ (s^{-1})	$k_{rigor\text{-}detach}$ (s^{-1})
23	23	4.4	4.4	100	100	1.5

Table S1. Rate constants used for initial force-free biochemical transitions of the model of Fig. 5. From (36) and 100 s^{-1} is an approximate starting point based on (35), the measured run length of the motor and the estimated ATP hydrolysis rate of >100 s^{-1} in (36))

Occupancy of the 15 states is represented by a vector of probabilities and a single state transition is simulated by multiplying the occupancy vector by the Markov matrix. The cumulative occupancies of each state in a run are determined by serial multiplication by the Markov matrix until the run terminates (i.e. the molecule enters state G). This is a geometric series from which the mean number of state occupancies can be calculated analytically. Run time is given by state dwell times multiplied by total occupancies of each state. The run length is determined by the net translocation (forward steps minus backwards steps) multiplied by the experimentally determined step size. The velocity is given by the average run length divided by the average run time.

The rate of ATP binding is proportional to the ATP concentration, and thus, velocity, run length, and fraction of backwards steps can be modeled as a function of [MgATP]. Starting with parameters determined by biochemical experiments (Table S3), the transition rates were varied manually to minimize the squared, standardized residual errors between the model run length, velocity, and backwards stepping experimental data, leading to the parameter values listed in text Table 2.

Supplemental Methods for smFRET experiments (Fig. S2):

Custom peptides from the coiled-coil portion of LZIPMX and APCCMX (Fig. S2A) with single cysteine mutations located on the outside of the coiled-coils were ordered from Life Tein LLC, USA. Peptides were labeled with a 1:1 ratio of Cy3 maleimide and Cy5 maleimide (Sigma-Aldrich USA) to obtain approximately 50% of dimers with a complementary FRET pair. Briefly, peptides were dissolved in labeling buffer, 25 mM Tris at pH 7.0, 100 mM NaCl, 2 mM EDTA, and 10 μM tris(2-carboxyethyl)phosphine, TCEP. Dyes were dissolved in DMF at a concentration of 0.9 mM before being added to the peptide with the labeling buffer, at a total 5:1 molar ratio of dye to peptide, 20 μM, and Cy3 maleimide and Cy5 maleimide 50 μM each. The reaction was allowed to proceed for 4 h and then quenched by adding sodium 2-mercaptoethanesulfonate, MESNA, to a final concentration of 3 mM. Dye was removed by 2 passes over G-25 spin columns.

An enzymatic deoxygenation system of 0.3% (w/v) glucose, 300 μg/ml glucose oxidase (Sigma-Aldrich), 120 μg/ml catalase (Roche), and 1.5 mM 6-hydroxy-2,5,7,8-tetramethyl-chromane-2-carboxylic acid (Trolox, Sigma-Aldrich) was added to M5 to form the final imaging buffer to reduce fluorophore photobleaching and blinking (44).

Cy3 and Cy5 fluorescence intensities were collected via alternating laser excitation (ALEX), switching between 532 nm and 640 nm laser excitation on an objective-type total internal reflection fluorescence microscope (43). Images were recorded at a 50 ms integration time, totaling for 100 ms frame rate and FRET traces were analyzed by custom analysis software (44), implemented in Matlab (Mathwords Inc.).

FRET efficiency was calculated according to:

$$E = \left(1 + \frac{I_D}{I_A - \chi I_D}\gamma\right)^{-1}$$

where I_D and I_A are the fluorescence intensities of the donor and acceptor minus background, χ is the cross-talk of the donor emission into the acceptor recording channel, and γ accounts for the ratios of quantum yield and detection efficiency between the donor and the acceptor channels (45). The distance between the donor (Cy3) and the acceptor (Cy5), *R*, can be determined from the FRET efficiency by the Förster equation:

$$E = \frac{1}{1 + \left(\frac{R}{R_0}\right)^6}$$

Where the Förster distance, R_0, for the Cy3-Cy5 FRET pair is 5.6 nm.

43. Jamiolkowski, R. M., Chen, C., Cooperman, B.S., Goldman, Y.E., 2017, tRNA Fluctuations Observed on Stalled Ribosomes Are Suppressed during Ongoing Protein Synthesis, Biophys. J. 113, 2326-2335.

44. Chen, C., Stevens, B., Kaur, J., Cabral, D., Liu, H., Wang, Y., Zhang, H., Rosenblum, G., Smilansky, Z., Goldman, Y.E., Cooperman, B.S., 2011. Single-Molecule Fluorescence Measurements of Ribosomal Translocation Dynamics, Mol. Cell, 42, 3, 367-377.

45. Roy, R., Hohng S., Ha, T., 2008, A Practial Guide to Single Molecule FRET, Nat. Methods, 5, 6, 507-516.